

**Very high column density and small reddening towards
GRB 020124 at $z = 3.20^1$**

J. Hjorth², P. Møller³, J. Gorosabel^{4,5,6}, J. P. U. Fynbo^{7,2}, S. Toft², A. O. Jaunsen⁸,
A. A. Kaas⁹, T. Pursimo⁹, K. Torii¹⁰, T. Kato¹¹, H. Yamaoka¹², A. Yoshida^{13,10},
B. Thomsen⁷, M. I. Andersen¹⁴, I. Burud⁶, J. M. Castro Cerón¹⁵, A. J. Castro-Tirado⁵
A. S. Fruchter⁶, L. Kaper¹⁶, C. Kouveliotou¹⁷, N. Masetti¹⁸, E. Palazzi¹⁸, H. Pedersen²,
E. Pian¹⁹, J. Rhoads⁶, E. Rol¹⁶, N. R. Tanvir²⁰, P. M. Vreeswijk⁸, R. A. M. J. Wijers¹⁶,
E. P. J. van den Heuvel¹⁶

ABSTRACT

We present optical and near-infrared observations of the dim afterglow of GRB 020124, obtained between 2 and 68 hours after the gamma-ray burst. The burst occurred in a very faint ($R \gtrsim 29.5$) Damped Ly α Absorber (DLA) at a redshift of $z = 3.198 \pm 0.004$. The derived column density of neutral hydrogen is $\log(N_{HI}) = 21.7 \pm 0.2$ and the rest-frame reddening is constrained to be $E(B - V) < 0.065$, i.e., $A_V < 0.20$ for standard extinction laws with $R_V \approx 3$. The resulting dust-to-gas ratio is less than 11% of that found in the Milky Way, but consistent with

²Astronomical Observatory, University of Copenhagen, Juliane Maries Vej 30, DK-2100 Copenhagen Ø, Denmark;

`jens@astro.ku.dk`

³European Southern Observatory, Karl-Schwarzschild-Strasse 2, D-85748 Garching bei München, Germany

⁴Danish Space Research Institute, Juliane Maries Vej 30, DK-2100 Copenhagen Ø, Denmark

⁵Instituto de Astrofísica de Andalucía (IAA-CSIC), Apartado 3.004, E-18080 Granada, Spain

⁶Space Telescope Science Institute, 3700 San Martin Drive, Baltimore, MD 21218

⁷Department of Physics and Astronomy, University of Aarhus, DK-8000 Århus C, Denmark

⁸European Southern Observatory, Casilla 19001, Santiago 19, Chile

⁹Nordic Optical Telescope, Apartado 474, E-38700 St. Cruz de La Palma, Canary Islands, Spain

¹⁰Cosmic Radiation Laboratory, RIKEN, 2-1, Hirosawa, Wako 351-0198, Japan

¹¹Department of Astronomy, Kyoto University, Sakyo-ku, Kyoto 606-8502, Japan

¹²Department of Physics, Faculty of Science, Kyushu University, Chuo-ku, Fukuoka 810-8560, Japan

¹³Department of Physics, Aoyama Gakuin University, 6-16-1, Chitosedai, Setagaya 157-8572, Japan

¹⁴Astrophysikalisches Institut Potsdam, D-14482 Potsdam, Germany

¹⁵Real Instituto y Observatorio de la Armada, Sección de Astronomía, 11.110 San Fernando-Naval (Cádiz), Spain

¹⁶Astronomical Institute ‘Anton Pannekoek’, NL-1098 SJ Amsterdam, The Netherlands

¹⁷Universities Research Association, Marshall Space Flight Center (NASA), Huntsville, AL 35812

¹⁸IASF/CNR, Sezione di Bologna, Via Gobetti 101, I-40129 Bologna, Italy

¹⁹INAF, Osservatorio Astronomico di Trieste, via Tiepolo, I-34131 Trieste, Italy

²⁰Department of Physical Sciences, University of Hertfordshire, College Lane, Hatfield, Hertfordshire AL10 9AB, UK

the SMC and high-redshift QSO DLAs, indicating a low metallicity and/or a low dust-to-metals ratio in the burst environment. A grey extinction law (large R_V), produced through preferential destruction of small dust grains by the GRB, could increase the derived A_V and dust-to-gas ratio. The dimness of the afterglow is however fully accounted for by the high redshift: If GRB 020124 had been at $z = 1$ it would have been approximately 1.8 mag brighter—in the range of typical bright afterglows.

Subject headings: cosmology: observations — dust, extinction — galaxies: abundances — galaxies: ISM — gamma rays: bursts

1. Introduction

Spectroscopy of the optical afterglows of cosmological GRBs allows detailed studies of the chemical and kinematical properties of gas along the lines of sight. Independently of the brightness of the host galaxy, the resulting insight into the GRB environment and its dust and gas content can provide clues to the nature of GRB progenitors as well as the properties of high-redshift galaxies. In particular, constraints on the column density of neutral hydrogen, $N(\text{H I})$, can be obtained through $\text{Ly}\alpha$ absorption if the burst is sufficiently distant to redshift the $\text{Ly}\alpha$ line into the near-UV/optical domain. Unlike X-ray studies where one infers $N(\text{H I})$ only indirectly based on an assumed metallicity, the derived $N(\text{H I})$ will be independent of metallicity.

In this regard, spectroscopy of GRB optical afterglows bears some resemblance to that of Damped $\text{Ly}\alpha$ Absorbers (DLAs, Wolfe et al. (1986)), which are gas-rich absorption systems intervening the lines of sight to background sources, such as QSOs. DLAs are chemically enriched and are therefore most likely caused by gas in, or close to, galaxies (e.g., Lu et al. (1996) and references therein; Pettini et al. (1997a)). In some cases galaxy counterparts of DLAs have been detected directly (Møller & Warren 1993, 1998; Djorgovski et al. 1996; Fynbo, Møller & Warren 1999; Møller et al. 2002). The important and interesting difference between QSO DLAs and GRB absorption systems is that the lines of sight through QSO

¹Based on observations with the Nordic Optical Telescope, which is operated on the island of La Palma jointly by Denmark, Finland, Iceland, Norway, and Sweden, at the Spanish Observatorio del Roque de los Muchachos of the Instituto de Astrofísica de Canarias, and on observations collected by the Gamma-Ray Burst Collaboration at ESO (GRACE) at the European Southern Observatory, Paranal, Chile (ESO Large Programme 165.H-0464)

DLAs are absorption cross-section selected whereas GRB absorbers (at the GRB redshift) are ‘GRB progenitor site’ selected. Therefore, GRB absorbers are likely to probe sightlines through different parts of DLA galaxies than QSO absorbers do, and hence contribute to a more complete picture of the properties of high-redshift galaxies.

The dust content of DLAs has been constrained mainly by two methods: i) by comparing the colors of background QSOs having intervening DLAs with the colors of a control sample of QSOs without intervening DLAs (Pei et al. 1991), and ii) by studying the metal abundance ratios, most notably Zn vs. Si and iron group elements, and inferring the dust depletion by comparison with interstellar clouds in the Galaxy (Lu et al. 1996; Kulkarni, Fall & Truran 1997; Pettini et al. 1997b; Ledoux, Bergeron & Petitjean 2002). The main conclusion of these studies is that DLAs in general are metal poor and that the fraction of the metals bound in dust grains is roughly the same as, or somewhat lower than, that found in the Galaxy.

This paper presents optical/near-IR photometry and optical spectroscopy of the afterglow of GRB 020124. GRB 020124 (burst trigger on Jan 24.44531 2002 UT) was the second *HETE-II* burst (Ricker et al. 2002) to be localized to arcsec precision and is the only burst for which a host galaxy has not been detected when searched for with *HST* (Berger et al. 2002; Bloom, Kulkarni & Djorgovski 2002). We determine the redshift of the burst to be 3.20, which is the fourth highest redshift known for a GRB to date, and the third highest (after GRB 000131 at $z = 4.50$ (Andersen et al. 2000) and GRB 030323 at $z = 3.37$ (Vreeswijk et al. 2003a)) based on afterglow absorption lines rather than host galaxy emission lines. We also show that it has a very high column density, qualifying it as a DLA (the highest value of $N(\text{H I})$ of known GRB afterglows and higher than almost all QSO DLAs). We discuss the implications for the dust-to-gas ratio of the GRB surroundings, including the effects of metallicity and destruction of dust by the GRB itself.

We assume a cosmology where $H_0 = 70 \text{ km s}^{-1} \text{ Mpc}^{-1}$, $\Omega_m = 0.3$, and $\Omega_\Lambda = 0.7$. For these parameters, a redshift of 3.20 corresponds to a luminosity distance of 27.47 Gpc and a distance modulus of 47.19. One arcsecond corresponds to 7.55 proper kpc, and the lookback time is 11.5 Gyr.

2. Observations

The observing log and photometric results are reported in Table 1 and summarized below.

2.1. Optical imaging

The position of the burst was observed at RIKEN with the 0.25 m f/3.4 hyperboloid astrograph equipped with unfiltered CCD camera AP7p. The field of view was $50' \times 50'$ which covered the entire $12'$ radius *HETE-II* error circle (Ricker et al. 2002). The observation started at Jan 24.530 UT; 126 frames of 20-s exposure were acquired by Jan 24.574 UT. PSF photometry was applied to each of the 126 frames. The resultant photometric measurements were combined to yield a 3.0σ detection at the position of the afterglow reported by Berger et al. (2002).

R-band images of the optical afterglow were obtained with StanCam at the 2.56 m Nordic Optical Telescope (NOT) between Jan 26.035 and Jan 26.076 2002 UT. I-band images were obtained at VLT-Melipal (UT3) between Jan 26.311 and 26.318 UT. R-band images were obtained with FORS1 on VLT-Melipal between Jan 27.278 UT and 27.292 UT. The latter images have a pronounced background pattern due to instrument reflections of the very bright background (the moon was $\sim 75\%$ illuminated). The variation in the pattern across the field is approximately 3–4 %. To flatten each individual image we used SExtractor to create a smoothed background image which was subsequently subtracted. The five background-subtracted images were then combined.

All images were preprocessed using standard tools and calibrated using nearby comparison stars from the field photometry of Henden (2002). The derived magnitudes are listed in Table 1.

2.2. Near-infrared imaging

Near-IR observations were obtained with ISAAC on VLT-Antu (UT1). The data consist of a total of 30 min in the Ks band and 30 min in the Js band obtained on Jan 26.2 UT and 30 min in the Ks band obtained on Jan 27.2 UT. The reduction was carried out with the “eclipse” software package (Devillard 1997) and the IRAF “Experimental Deep Infrared Mosaicing Software” xdimsum. Eclipse was used to remove effects of electrical ghosts from science and calibration frames and to construct flat fields and bad-pixel maps from a series of twilight-sky flats. Sky subtraction and combination of the dithered science frames were carried out with xdimsum. To account for the rapidly varying background, the sky value in each pixel was calculated as the running median of the pixel value in the exposures taken immediately before and after a given exposure. To minimize the effects on the running median of bright objects in neighboring frames, the subtraction was carried out in two iterative steps: First, a cosmic-ray cleaned, background-subtracted combined image was constructed from which a

mask of all the objects was created. This mask was then registered to the individual frames and taken into account in the following running median background subtraction. Residual background signatures were subsequently removed by fitting high-order polynomials to the rows and columns of the individual (masked) frames. Finally, the individual background-subtracted images were registered and median combined. Excerpts of the resulting images are shown in Fig. 1.

Photometric calibration to J and Ks magnitudes was performed using standard star observations of 9106/S301–D and 9149/S860–D (Persson et al. 1998) on the nights of observation. The images were astrometrically calibrated using comparison stars from the Guide Star Catalogue II (GSC-II)²¹ using the WCStools software package by D. Mink²². The absolute astrometry has an rms of $0''.43$ in the Ks band. The resulting coordinates of the infrared afterglow of GRB 020124 are R.A. (J2000.0) = $09^h32^m50.82^s$, Dec. (J2000.0) = $-11^\circ31'11''.0$, consistent with the position of the radio and optical afterglow (Berger et al. 2002).

2.3. Spectroscopy

Spectroscopic observations were obtained on Jan 26.3 with FORS1 on VLT-Melipal using the 300V+10 grism and the order-separation filter GG375 in long-slit mode with a 1.0 arcsec wide slit. This configuration provides a wavelength coverage $3650 - 7500 \text{ \AA}$ at a resolution of 13 \AA . The total integration time was 1200 sec, evenly divided between two exposures. Standard data reduction procedures were performed using MIDAS. The two separate exposures allowed us to reliably reject cosmic-ray events before co-addition. The spectrophotometric standard LTT9491 (Hamuy et al. 1994) was observed using the same configuration.

²¹The Guide Star Catalogue II is a joint project of the Space Telescope Science Institute and the Osservatorio Astronomico di Torino. Space Telescope Science Institute is operated by the Association of Universities for Research in Astronomy, for the National Aeronautics and Space Administration under contract NAS5-26555. The participation of the Osservatorio Astronomico di Torino is supported by the Italian Council for Research in Astronomy. Additional support is provided by European Southern Observatory, Space Telescope European Coordinating Facility, the International GEMINI project and the European Space Agency Astrophysics Division.

²²<http://tdc-www.harvard.edu/TDC.html>

3. Results

3.1. Spectral energy distribution: spectral index and redshift estimate

The extracted, flux calibrated spectrum is shown in Fig. 2. Due to the faintness of the object spectrum and the resulting dominance of systematic errors from sky subtraction close to bright airglow lines, the signal-to-noise fluctuates rapidly in the red part of the spectrum. What may look like absorption or emission features redwards of 5500 Å should therefore not be trusted. The strong absorption line around 5100 Å is clearly significant, and several other absorption features bluewards of 5500 Å are marginally significant at the 3–4 σ level.

One or more of the absorption lines seen in the blue part of Fig. 2 could be due to Ly α , which would indicate a redshift in excess of 2.3. Our first objective was therefore to construct the spectral energy distribution (SED) in the optical to determine its slope, and to look for possible large-scale signatures (spectral drops) which might indicate the onset of the Lyman Forest and/or the Lyman Valley as expected in an object with redshift significantly in excess of 2.3. For this purpose we carefully defined a series of intervals along the spectrum where systematic errors from night-sky emission-line subtraction did not pose any problems. The total number of counts was determined in each interval of the afterglow spectrum as well as of the spectrum of the spectrophotometric standard. Uncertainties were calculated directly via propagation of photon statistics.

The resulting fluxes and corresponding uncertainties (after correction for airmass) in each bin are plotted in Fig. 3. In Fig. 3a the minimum- χ^2 pure power-law fit ($f_\nu \propto \nu^{-\beta}$; $\beta = 2.36 \pm 0.23$; reported uncertainties are 1σ errors throughout this paper) is overplotted, but is seen to be a very poor fit to the data points. In particular the data point at 5100 Å falls many standard deviations below any power-law fit. Such a large drop in that wide a bin can effectively only be caused by a damped Ly α line at a redshift of about 3.2. At this redshift one expects to see not only the Ly α line but also a significant drop due to the Lyman Forest, and the signature of the onset of the red slope of the Lyman Valley (Møller & Jakobsen 1990). In Fig. 3b we therefore plot the same data points, but here we overlay a model power law including the predicted absorption due to the intervening intergalactic medium at $z = 3.2$. The power law again represents the minimum- χ^2 fit and has an index of $\beta = 1.32 \pm 0.25$. Comparing the χ^2 of the fits in Fig. 3a and Fig. 3b, we find that even if we ignore the presence of the Ly α line (i.e. consider only the large-scale SED), the $z = 3.2$ model SED represents an acceptable fit while the pure power law is rejected at the 98.6 % confidence level ($\Delta\chi^2 = 16.4$ for 20 degrees of freedom (dof)).

3.2. Redshift and H I column density of the Ly α line

Following the determination of the underlying power-law index and approximate redshift, we proceeded to fit the Ly α line itself. The part of the spectrum useful for line-fitting is shown again in Fig. 4, here normalized by division with the fitted power-law. Overplotted are model absorption spectra with $z = 3.198$. The model spectra include the Lyman series, Si II, Si III, and O I lines. On the blue side of the Ly α line we see the expected line-blanketing by the Lyman Forest. At this resolution, lines in the Lyman Forest are therefore not useful for a precise redshift determination, and we shall rely only on the Si II $\lambda 1260$ and O I $\lambda 1302$ lines at 5294 Å and 5468 Å for this purpose. The first line is an unblended Si II $\lambda 1260$ line providing a best-fit redshift of 3.200 ± 0.004 . The O I $\lambda 1302$ line is blended with a much weaker Si II $\lambda 1304$ line and provides a redshift of 3.196 ± 0.004 . The combined redshift of these two lines, including wavelength calibration errors, is $z_{\text{metal}} = 3.198 \pm 0.004$ which we shall adopt as the systemic redshift of the absorber.

Because of the line-blanketing on the blue side of the Ly α line, only the red part of the line profile could be used to constrain the H I column density of the absorber. Within the uncertainty of the redshift we found that acceptable fits could be obtained in the range $\log(N_{\text{HI}}) = 21.7 \pm 0.2$. The estimated 1σ range is marked in Fig. 4 as dotted lines. This column density is among the very highest values observed for QSO DLAs (Storrie-Lombardi & Wolfe 2000). The absorption system is unlikely to be “intervening” (i.e. unrelated to the GRB host) because of the very small probability of such a high-column-density intervening absorber. More importantly, a significantly higher redshift of the GRB is ruled out by the lack of even stronger Lyman Forest absorption redward of 5200 Å (Fig. 3).

3.3. Characteristics of the optical decay

In addition to the data presented here, we include the data reported by Berger et al. (2002) to constrain the R-band lightcurve. In Fig. 5 we plot all the R-band data points vs. the logarithm of time since the GRB. The power-law decay index derived from a weighted fit to all the data is $\alpha = 1.64 \pm 0.03$ ($f_{\nu} \propto (t - t_{\text{GRB}})^{-\alpha}$). This fit is formally rejected with a reduced $\chi^2/\text{dof} = 26/14$. Excluding the late-time HST data we derive an acceptable fit with a decay index of $\alpha = 1.49 \pm 0.04$ and $\chi^2/\text{dof} = 6/12$. Fitting only to the data prior to 1 day after the burst we derive a decay index of $\alpha = 1.45 \pm 0.06$ with $\chi^2/\text{dof} = 5/10$. These results confirm the conclusion of Berger et al. (2002) that the lightcurve is becoming progressively steeper (a ‘break’) (see Fig. 5).

3.4. Optical/near-infrared SED

Assuming a power-law decay index $\alpha = 1.49 \pm 0.04$ we can interpolate the RIJKs-band data taken around Jan. 26 UT to a common epoch at Jan 26.20 2002 UT. After dereddening the contemporaneous RIJKs-band points for Galactic extinction (Schlegel, Finkbeiner & Davis 1998), the colors are $R - K_s = 2.93 \pm 0.26$ and $J - K_s = 1.33 \pm 0.20$. These colors are consistent with the ones expected of a GRB afterglow (see the shaded region of the color-color diagram in Fig. 2 of Gorosabel et al. (2002a)).

We have used the intrinsic spectral index obtained from the VLT spectrum ($\beta = 1.32 \pm 0.25$, see § 3.1) to obtain a mock B-band point by a power-law extrapolation of the R-band measurement. In order to infer information on the extinction (A_V , $E(B-V)$), the BRIJKs-band SED was fitted with a functional form $f_\nu \propto \nu^{-\beta} \times 10^{-0.4A_\nu}$, where A_ν is the extinction in magnitudes at rest-frame frequency ν . A_ν was parametrized in terms of A_V using the three extinction laws reported by Pei (1992), i.e., for the Small Magellanic Cloud (SMC), Large Magellanic Cloud (LMC) and for the Milky Way (MW). For comparison purposes we also considered the unextinguished case (pure power law spectrum given by $f_\nu \propto \nu^{-\beta}$).

As shown in Fig. 6 and Table 2 (third column) the fits of the three extinction laws are consistent with the data. The derived extinctions are consistent with the no-extinction case (in which case $\beta = 0.91 \pm 0.14$). Based on these fits we can set an upper limit of $E(B - V) < 0.18$. This upper limit however corresponds to an unrealistic value of β . Constraining the spectral index to be $\beta > 0.5$ and the extinction law to be that of the SMC (which provides the best fit to this and most other afterglow SEDs) we find that $E(B - V) < 0.065$. The β values derived for the three extinguished cases agree with the pure power-law case.

4. Discussion

4.1. Jet-wind fireball model

Within the framework of the afterglow synchrotron model (Sari, Piran & Narayan 1998), the decay index, α , and the spectral index, β , are related through the slope of the electron energy distribution, p . Given the low extinction inferred from the SED analysis we find that a jet ($\nu < \nu_c$, the synchrotron cooling frequency) expanding into a wind medium ($n \propto r^{-2}$) provides the best fireball model for the data. For $\alpha_1 = 1.49 \pm 0.04$, this model requires $p = 2.32 \pm 0.05$, and $\beta = 0.66 \pm 0.03$, consistent with the observational results with modest extinction. Expansion into a homogeneous medium ($\nu < \nu_c$) is not strictly ruled out but requires an unusually high value of p : the predicted values are $p = 2.99 \pm 0.05$ and

$\beta = 1.00 \pm 0.03$ (for $\alpha_1 = 1.49 \pm 0.04$), consistent with the observational values in the absence of extinction.

4.2. How robust is the redshift determination?

The spectrum has low resolution and signal-to-noise ratio, but there are five independent pieces of evidence for the redshift. First, assuming a pure power-law for the spectrum provides a spectral index of 2.36 ± 0.23 which is incompatible with $\beta = 0.91 \pm 0.14$ determined from the photometry. Second, the strong absorption line at 5100 \AA cannot be explained by anything else than $\text{Ly}\alpha$ at a redshift around 3.2. Third, assuming $z = 3.2$ and fitting a model with free spectral index but now including the predicted Lyman Forest and Valley absorption, one obtains a minimum- χ^2 fit for a spectral index of 1.32 ± 0.25 which is fully compatible with the photometric determination. Fourth, the $z = 3.2$ fit leads to an improvement in χ^2 over a single power-law alone (for the same degrees of freedom) which rejects the single power-law at the 98.6 % level. Fifth, there are two identified metal lines, and none of the lines predicted from the explicit fit (e.g. $\text{Ly}\beta$) are inconsistent with the observed spectrum (Fig. 4).

4.3. Dim or bright?

The fact that GRB 020124 was a fairly dim burst (Berger et al. 2002), but fitted by a normal fireball model without excessive extinction reinforces the conclusion of Hjorth et al. (2002) (GRB 980613), Berger et al. (2002) (GRB 020124), and Fox et al. (2003) (GRB 021211) that there is a population of dim, unextinguished GRB afterglows that can account for at least some of the large fraction of (‘dark’) bursts for which no optical afterglow is detected (Fynbo et al. 2001a). In the case of GRB 020124 this is mainly due to the fairly high redshift (unlike GRB 980613 and GRB 021211 which are at redshifts 1.096 (Djorgovski et al. 1999) and 1.006 (Vreeswijk et al. 2003b), respectively): If an afterglow is redshifted from z_1 to z_2 it is dimmed by $\Delta\mu + 2.5(\beta - \alpha - 1) \log((1 + z_2)/(1 + z_1))$. For a median GRB redshift of $z_1 = 1$ and $z_2 = 3.198$ the relative dimming amounts to 1.82 mag (for $\alpha = 1.49$ and $\beta = 0.91$). If the afterglow had been 1.82 mag brighter it would have been a typical bright afterglow: $R \approx 16.7$ after two hours and $R \approx 20.7$ after one day (see e.g. Fig. 3 of Gorosabel et al. (2002b) or Fig. 2 of Fox et al. (2003)).

4.4. N(H I) vs. E(B–V)

The Galactic relation between the column density of neutral hydrogen and the reddening is $N(\text{H I})/E(\text{B–V}) = 4.93 \pm 0.28 \times 10^{21} \text{ cm}^2 \text{ mag}^{-1}$ (Diplas & Savage 1994). For the LMC and SMC the corresponding ratios are $N(\text{H I})/E(\text{B–V}) = 2 \pm 0.5 \times 10^{22} \text{ cm}^2 \text{ mag}^{-1}$ and $N(\text{H I})/E(\text{B–V}) = 4.4 \pm 0.7 \times 10^{22} \text{ cm}^2 \text{ mag}^{-1}$, respectively (Koornneef 1982; Bouchet et al. 1985). In Table 3 we list this ratio for known GRBs for which the H I column density and E(B–V) have been measured or constrained from optical spectroscopy and optical/near-infrared photometry (the values given are for an SMC extinction law). In addition to GRB 020124 these are GRB 000301C (Jensen et al. 2001) and GRB 000926 (Fynbo et al. 2001b,c). We exclude GRB 021004 which has several intervening absorbers at different redshifts. It is evident that the values for $N(\text{H I})/E(\text{B–V})$ are not larger than expected for galaxies like the LMC or SMC. Taken at face value these results indicate that the GRB surroundings are low in dust, because of low metallicity (e.g., for a universal dust-to-metals ratio) and/or because of a low dust-to-metals ratio (a large fraction of the metals being in the gas phase). This conclusion is fully consistent with what is found in QSO DLAs (Pettini et al. 1997b).

It has been suggested that the intense UV and X-ray flux from a GRB may photoionize the surrounding gas and destroy dust grains (Waxman & Draine 2000; Fruchter, Krolik & Rhoads 2001; Perna & Lazzati 2002), resulting in changes in the derived $N(\text{H I})$, A_V , $E(\text{B–V})$, and their ratios. Galama & Wijers (2001) studied the inferred absorption of soft X-rays in BeppoSAX GRB afterglows and compared it to the optical extinction as inferred from a fireball model fit to the available data. They claimed evidence for a high $N(\text{H I})/A_V$ ratio and concluded that dust destruction may be the cause. The most convincing case for dust destruction along these lines was made by Galama et al. (2003) who found a high value of $N(\text{H I})/A_V$ for GRB 010222, based on *Chandra X-ray Observatory* data. At the same time they interpreted a strong (i.e., non-grey) far-ultraviolet (restframe wavelength $\sim 1100 \text{ \AA}$) component in the extinction of GRB 010222 as evidence for dust destruction.

In a comparison of the properties of DLAs and GRB absorbers, Savaglio, Fall & Fiore (2003) claimed that GRB 990123 ($z = 1.60$), GRB 000926 ($z = 2.04$), and GRB 010222 ($z = 1.48$) (of which only GRB 000926 has a measured $N(\text{H I})$ (Fynbo et al. 2001b)) have higher metal column densities and contain more dust than DLAs at similar redshifts. They further suggested that the relatively low reddening (restframe wavelength $> 1200 \text{ \AA}$) observed towards these GRBs may be due to a grey extinction law, produced by dust destruction (Perna, Lazzati & Fiore 2003).

Castro et al. (2003) argue that the chromium-to-zinc ratio towards GRB 000926 indicates that the host is depleted in dust relative to local values to a similar degree as QSO DLAs at the same redshift. This conclusion is consistent with what we have suggested above

for GRB 020124, namely that the GRB surroundings have a low dust-to-gas ratio, similar to QSO DLAs (Pettini et al. 1997b). An additional argument in favor of this interpretation is that a significant amount of grey extinction would make the afterglow intrinsically even brighter than indicated above (§4.3). For example, assuming a Galactic value of $N(\text{H I})/A_V$, $\log N(\text{H I}) = 21.7$, destruction of 2/3 of the dust producing the extinction in the rest-frame V band (Perna, Lazzati & Fiore 2003) and a flat extinction curve would dim the afterglow by 1 mag. Any non-grey component would significantly increase this value.

We conclude that the high value of the ratio between column density and optical extinction first found by Galama & Wijers (2001) from X-ray spectroscopy remains when $N(\text{H I})$ is estimated from optical spectroscopy in GRB afterglows with a DLA host and the extinction is estimated from the observed reddening of the optical/NIR afterglow. The dust destruction interpretation originally proposed by Galama & Wijers (2001) to account for the X-ray result could conceivably also be applied in this case. The observed small reddening would be due to a modification of the extinction law due to preferential destruction of small grains by the prompt UV and X-ray radiation from the GRB, leading to a grey extinction law. However, we have found that the straightforward alternative explanation, namely that GRBs occur in less chemically enriched environments, similar to those of the SMC and QSO DLAs, is fully consistent with the optical observations reported here. Future joint optical and X-ray spectroscopy of $1.6 \lesssim z \lesssim 2.5$ GRBs combined with accurate multi-wavelength observations of the afterglow, in particular in the optical/NIR regime, can be used to distinguish between these two possibilities and at the same time fix the metallicity of the burst environment.

We thank Jochen Greiner, Sylvio Klose, and Kristian Pedersen for useful comments. JPUF acknowledges support from the Carlsberg Foundation. JMCC acknowledges the receipt of a FPI doctoral fellowship from Spain’s Ministerio de Ciencia y Tecnología. The authors acknowledge benefits from collaboration within the EU FP5 Research Training Network “Gamma-Ray Bursts: An Enigma and a Tool”. This work was also supported by the Danish Natural Science Research Council (SNF).

REFERENCES

- Andersen, M. I., et al. 2000, *A&A*, 364, L54
- Bessel, M. S. 1990, *PASP*, 102, 1181
- Berger, E., et al. 2002, *ApJ*, 581, 981
- Bloom, J. S., Kulkarni, S. R., & Djorgovski, S. G. 2002, *AJ*, 123, 1111
- Bouchet, P., Lequeux, J., Maurice, E., Prevot, L., & Prevot-Burnichon, M. L. 1985, *A&A*, 149, 330
- Castro, S., Galama, T. J., Harrison, F. A., Holtzman, J. A., Bloom, J. S., Djorgovski, S. G., & Kulkarni, S. R. 2003, *ApJ*, 586, 128
- Devillard, N. 1997, *The Messenger*, 87, 19
- Diplas, A., & Savage, B. D. 1994, *ApJ*, 427, 274
- Djorgovski, S. G., Pahre, M. A., Bechtold, J., & Elston, R. 1996, *Nature*, 382, 234
- Djorgovski, S. G., Kulkarni, S. R., Bloom, J. S., Frail, D., Chaffee, F., & Goodrich, R. 1999, *GCNC*, 189
- Fox, D. W., et al. 2003, *ApJ*, 586, L5
- Fruchter, A. S., Krolik, J. H., & Rhoads, J. E. 2001, *ApJ*, 563, 597
- Fynbo, J. P. U., Møller, P., & Warren, S. J. 1999, *MNRAS*, 305, 849
- Fynbo, J. P. U., et al. 2001a, *A&A*, 369, 373
- Fynbo, J. P. U., et al. 2001b, in *Lighthouses of the Universe: The Most Luminous Celestial Objects and Their Use for Cosmology*, Proc. of the MPA/ESO/MPE/USM Joint Astronomy Conf., eds. M. Gilfanov, R. Sunyaev, & E. Churazov (Garching: Springer), p. 187
- Fynbo, J. P. U., et al. 2001c, *A&A*, 373, 70
- Galama, T. J., & Wijers, R. A. M. J., 2001, *ApJ*, 549, L209
- Galama, T. J., et al. 2003, *ApJ*, 587, 135
- Gorosabel, J., et al. 2002a, *A&A*, 384, 11

- Gorosabel, J., et al. 2002b, *A&A*, 383, 112
- Hamuy, M., Suntzeff, N. B., Heathcote, S. R., Walker, A. R., Gigoux, P., & Phillips, M. M. 1994, *PASP*, 106, 566
- Henden, A. 2002, *GCNC*, 1251
- Hjorth, J., et al. 2002, *ApJ*, 576, 113
- Jensen, B. L., et al. 2001, *A&A*, 370, 909
- Koornneef, J. 1982, *A&A*, 107, 247
- Kulkarni, V. P., Fall, S. M., & Truran, J. W. 1997, *ApJ*, 484, L7
- Ledoux, C., Bergeron, J., & Petitjean, P. 2002, *A&A*, 385, 802
- Lu, L., Sargent, W. L. W., Barlow, T. A., Churchill, C. W., & Vogt, S. S. 1996, *ApJS*, 107, 475
- Møller, P., & Jakobsen, P. 1990, *A&A*, 228, 299
- Møller, P., & Warren, S. J. 1993, *A&A*, 270, 43
- Møller, P., & Warren, S. J. 1998, *MNRAS*, 299, 661
- Møller, P., Warren, S. J., Fall, S. M., Fynbo, J. P. U., & Jakobsen, P. 2002, *ApJ*, 574, 51
- Pei, Y. C., Fall, S. M., & Bechtold, J. 1991, *ApJ*, 378, 6
- Pei, Y. C. 1992, *ApJ*, 395, 130
- Perna, R., & Lazzati, D. 2002, *ApJ*, 580, 261
- Perna, R., Lazzati, D., & Fiore, F. 2003, *ApJ*, 585, 775
- Persson, S. E., Murphy, D. C., Krzeminski, W., Roth, M., & Rieke, M. J., *AJ*, 116, 2475
- Pettini, M., Smith, L. J., King, D. L., & Hunstead, R. W. 1997a, *ApJ*, 486, 665
- Pettini, M., King, D. L., Smith, L. J., & Hunstead, R. W. 1997b, *ApJ*, 478, 536
- Ricker, G. R., et al. 2002, *GCNC*, 1220
- Sari, R., Piran, T., & Narayan, R. 1998, *ApJ*, 497, L17
- Savaglio, S., Fall, S. M., & Fiore, F. 2003, *ApJ*, 585, 638

Schlegel, D. J., Finkbeiner, D. P., & Davis, M. 1998, ApJ, 500, 525

Storrie-Lombardi, L. J., & Wolfe, A. M. 2000, ApJ, 543, 552

Vreeswijk, P., Wijers, R., Rol, E., & Hjorth, J. 2003a, GCNC, 1953

Vreeswijk, P., Fruchter, A., Hjorth, J., & Kouveliotou, C. 2003b, GCNC, 1785

Waxman, E., & Draine, B. T. 2000, ApJ, 537, 796

Wolfe, A. M., Turnshek, D. A., Smith, H.E., & Cohen, R. D. 1986, ApJS, 61, 249

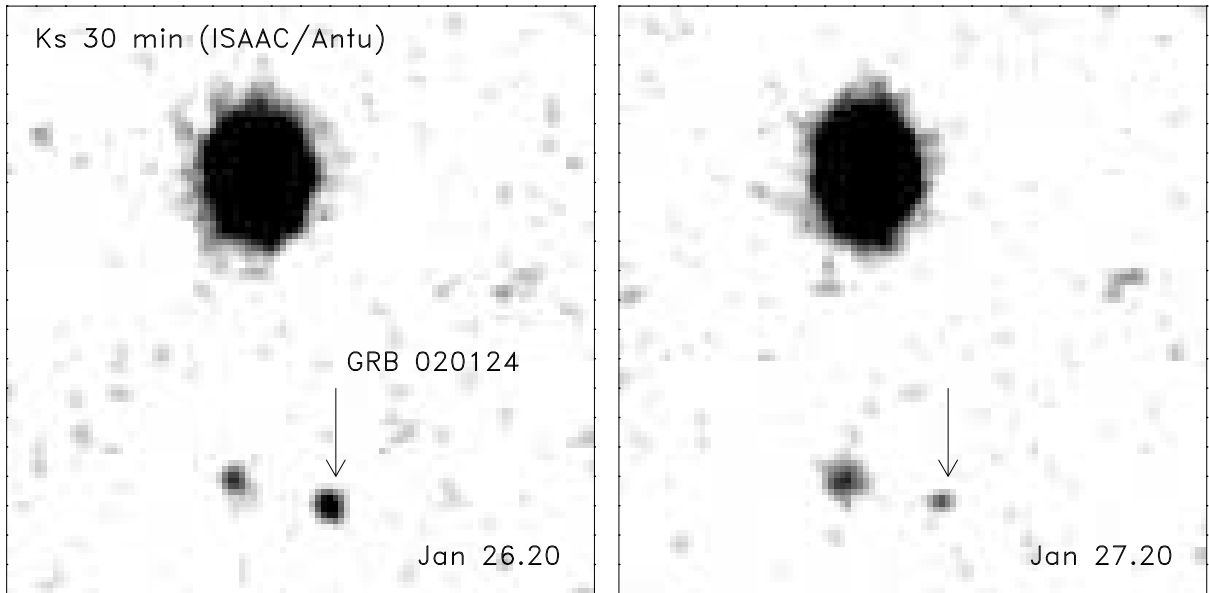


Fig. 1.— Ks images obtained with ISAAC on 2002 Jan 26.20 UT (left) and 27.20 UT (right) of GRB 020124 marked by an arrow. The images are $15'' \times 15''$. North is up and east is to the left.

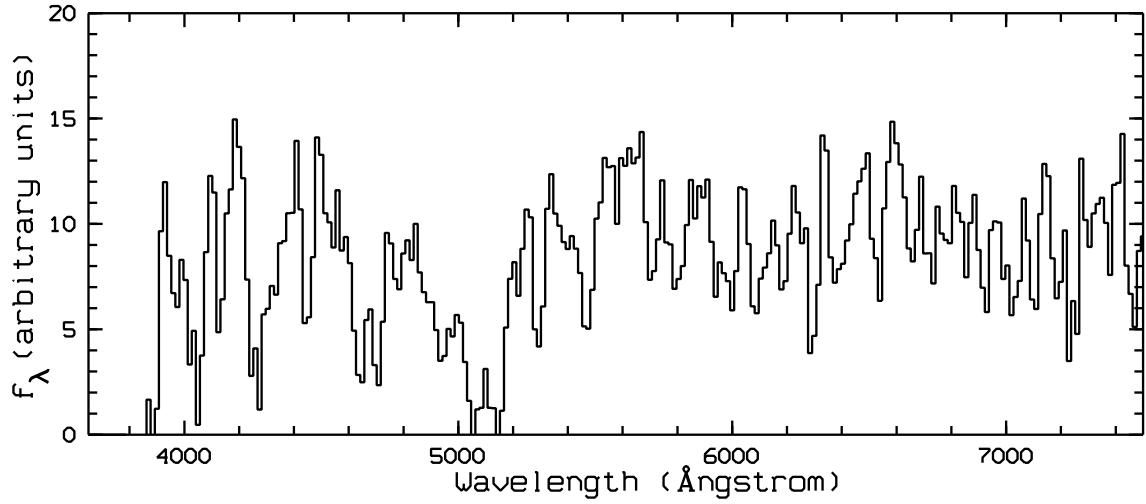


Fig. 2.— Extracted, flux calibrated FORS1 300V spectrum of GRB 020124 obtained on 2002 Jan 26.34 UT. The ordinate is f_λ in arbitrary units. From 4000 Å to 5500 Å the signal-to-noise ratio per resolution element (13 Å) in the continuum grows from 1.8 to 3.5. Longwards of 5500 Å the signal-to-noise ratio is completely dominated by sky-subtraction errors and therefore varies rapidly from pixel to pixel. In order to obtain the best possible value for the spectral slope of the spectrum we have identified “good” sections of the spectrum as detailed in § 3.1 and shown in Fig. 3.

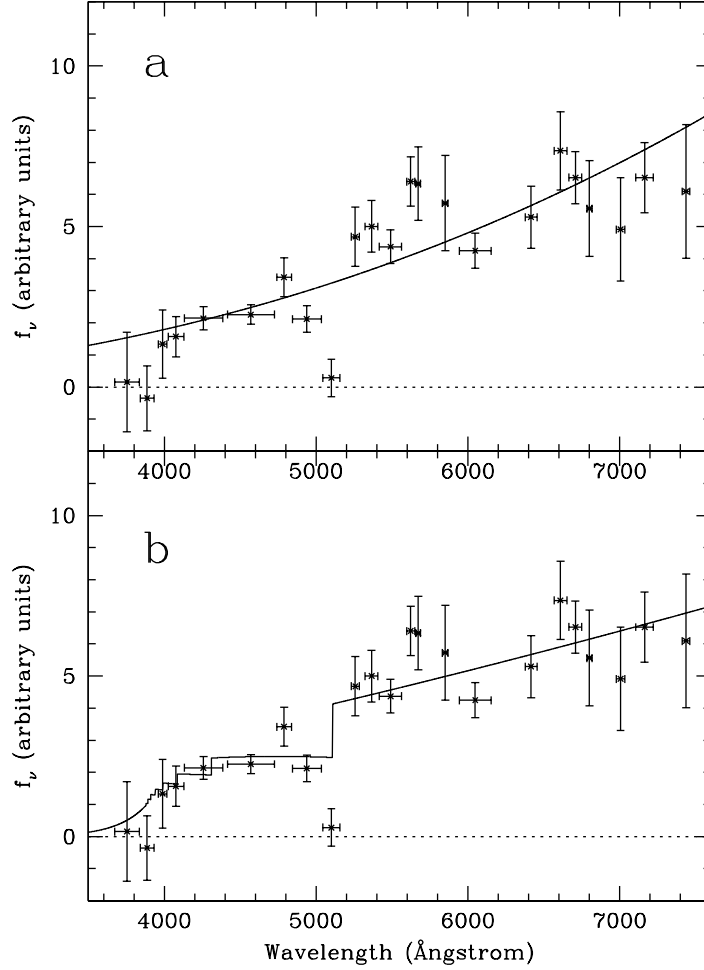


Fig. 3.— Spectrum of GRB 020124 (Fig. 2) summed in bins free from strong sky lines. (a) A pure power-law does not provide an acceptable fit mostly due to the strong absorption line at 5100 Å. This strong absorption feature can only be explained by a damped Ly α line close to $z = 3.2$. A power-law fit to the data excluding the bin at 5100 Å leads to a spectral slope of $\beta = 2.36 \pm 0.23$ incompatible with the optical/near-IR imaging. (b) A power-law fit including the effect of the Lyman Forest and Lyman Valley for a source redshift of $z = 3.198$ again omitting the bin at 5100 Å. The pure power-law fit (a) is rejected at the 98.6 % confidence level. The power-law slope of $\beta = 1.32 \pm 0.25$ resulting from the absorbed model fit (b) is consistent with the slope derived from the optical/near-IR imaging ($\beta = 0.91 \pm 0.14$).

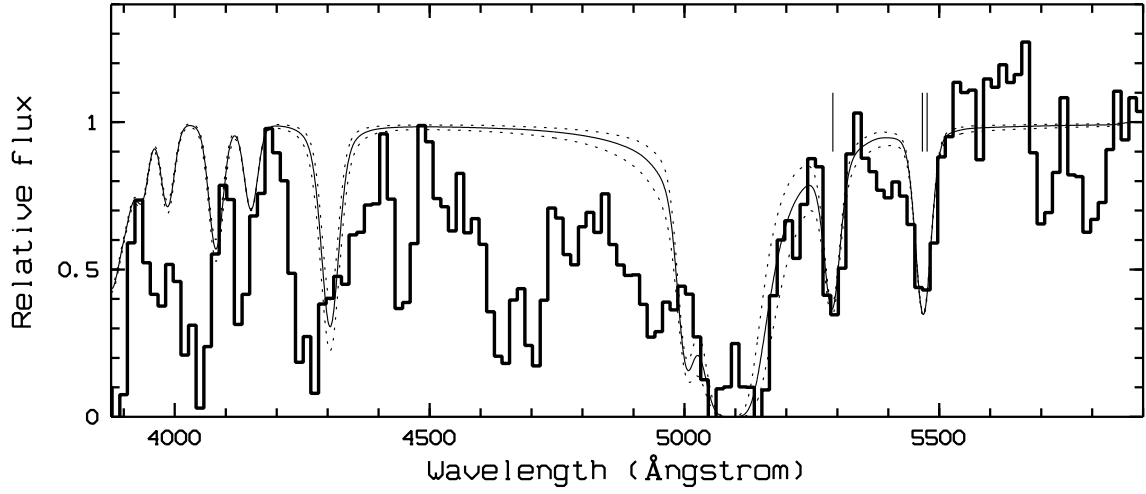


Fig. 4.— FORS1 300V spectrum and model overlay (solid curve) of a $z = 3.198$ damped $\text{Ly}\alpha$ line yielding $\log(N_{HI}) = 21.7 \pm 0.2$. The estimated 1σ range is plotted as dotted lines. The model has been fit to the red wing of the $\text{Ly}\alpha$ line and the two lines redward of it. These metal lines, identified as $\text{Si II } \lambda 1260$ and $\text{O I } \lambda 1302$ at 5294 \AA and 5468 \AA , were used for the redshift determination. For illustrative purposes we also show the region blueward of the $\text{Ly}\alpha$ line. This region is dominated by Lyman Forest absorption; the data are of very low signal-to-noise. The predicted model is also shown but is not fit to the data in this region. The data are consistent with the model considering the effect of Lyman Forest absorption.

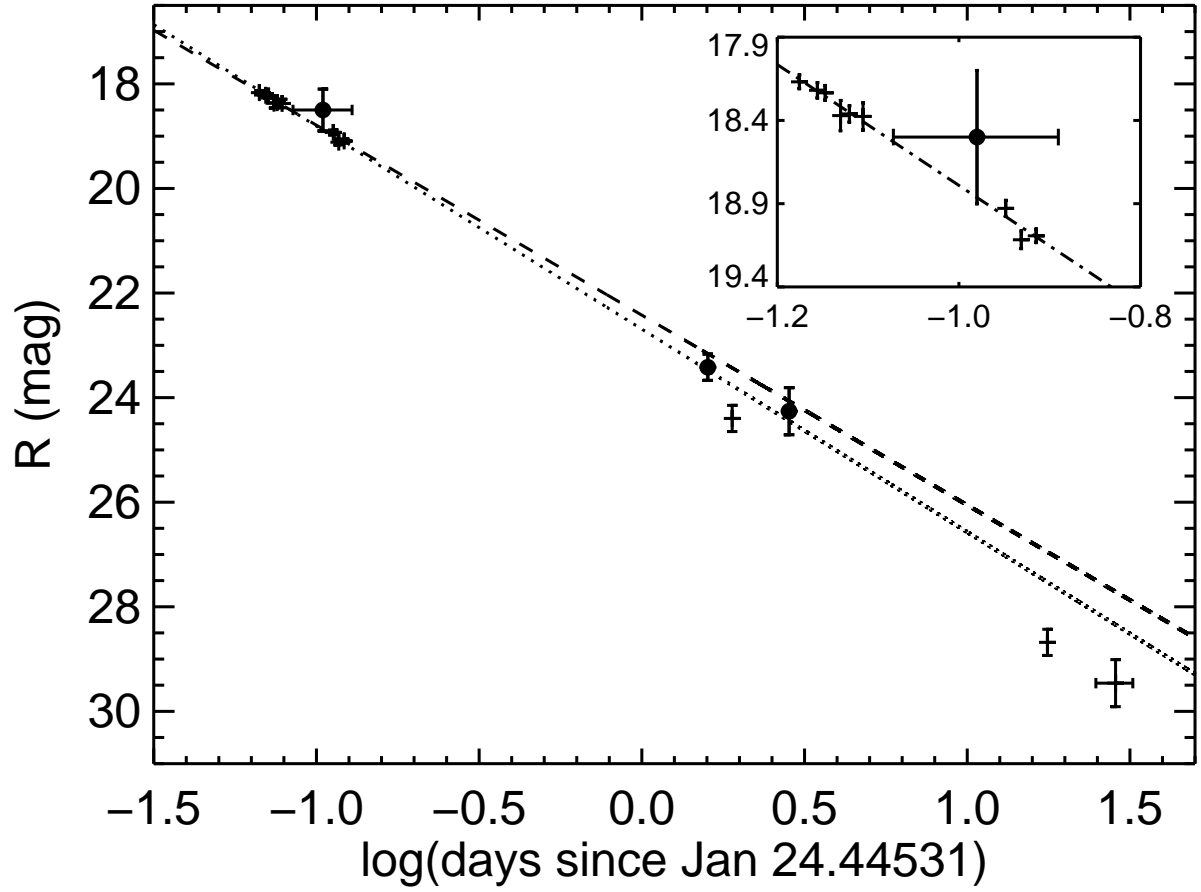


Fig. 5.— The R-band lightcurve based on our data (filled circles) and from Berger et al. (2002). The dashed line shows a fit to the early data points only. The dotted line is the result of a fit including also the two points from 1 to 3 days after the burst.

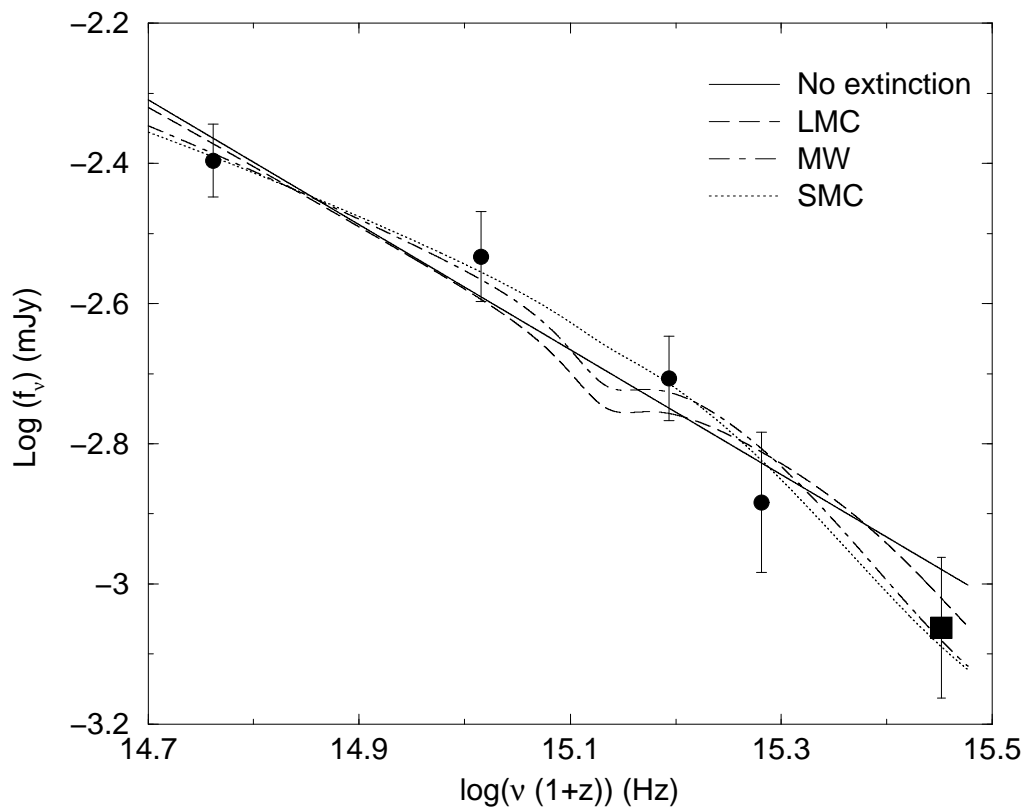


Fig. 6.— The BRIJKs-band spectral energy distribution of the afterglow on Jan 26.20 2003 UT. The filled circles represent the RIJKs-band measurements. The filled square is the fiducial B-band photometric point obtained by extrapolating the R-band point using the intrinsic spectral slope ($\beta = 1.32 \pm 0.25$) derived from the VLT spectrum. The fluxes have been corrected for Galactic extinction (Schlegel, Finkbeiner & Davis 1998). The frequencies are given in the rest frame for $z = 3.198$.

Table 1. Log of observations and photometry of the afterglow of GRB 020124

Date (Jan 2002 UT)	Filter ^a /Grism	Exposure time (sec)	Telescope ^b	FWHM ^c (arcsec)	Brightness ^d (mag)
24.55	unfiltered	126 × 20	RIKEN	2.2	18.5 ^{+0.4} _{-0.3}
26.04	R	6 × 600	NOT	1.14	23.42 ± 0.25
26.20	Ks	30 × 60	Antu	0.50	20.55 ± 0.13
26.23	Js	20 × 90	Antu	0.68	21.94 ± 0.16
26.32	I	2 × 60 + 120	Melipal	0.74	22.94 ± 0.15
26.34	300V	2 × 600	Melipal	1.2	
27.20	Ks	30 × 60	Antu	0.56	21.92 ^{+0.37} _{-0.28}
27.28	R	5 × 180	Melipal	0.66	24.26 ^{+0.45} _{-0.32}

^aThe broad-band optical (R, I) filters used were Bessel filters (Bessel 1990).

^bRIKEN represents a 0.25 m f/3.4 hyperboloid astrograph (Wako, Saitama, Japan) equipped with an unfiltered CCD camera; NOT is the 2.56 m Nordic Optical Telescope (La Palma, Canary Islands, Spain) equipped with StanCam; Antu and Melipal are the 8.2 m Unit Telescopes 1 and 3 on ESO’s VLT at Paranal Observatory, Chile, equipped with ISAAC and FORS1, respectively.

^cMeasured seeing full width at half maximum of point-like objects in the field.

^dUncorrected for Galactic extinction. The brightnesses are reported as R_C , I_C , J, Ks magnitudes.

Table 2. SED fitting results

Extinction law	χ^2/dof	E(B–V)	β
MW	1.22	0.045±0.101	0.69±0.50
LMC	0.56	0.098±0.079	0.29±0.52
SMC	0.31	0.071±0.051	0.31±0.43
No extinction	0.78	0	0.91±0.14

Table 3. Column density and reddening for GRB absorbers

GRB	z	$\log N(\text{H I})$	$E(\text{B}-\text{V})$ (mag)	$N(\text{H I})/E(\text{B}-\text{V})$ ($10^{21} \text{ cm}^2 \text{ mag}^{-1}$)	Reference
000301C	2.040	21.2 ± 0.5	0.031 ± 0.014	51_{-42}^{+113}	Jensen et al. 2001
000926	2.038	21.3 ± 0.2	0.062 ± 0.020	32_{-16}^{+21}	Fynbo et al. 2001b,c
020124	3.198	21.7 ± 0.2	< 0.065	> 49	this paper